DOI: 10.1002/ejic.200700400

Kinetics and Magnetism of Phosphane Diadducts of Diruthenium(II,III) Tetraacetate

Tara J. Burchell,[a] T. Stanley Cameron,[b] Donal H. Macartney,[c] Laurence K. Thompson,[d] and Manuel A. S. Aquino*[a]

Keywords: Carboxylate ligands / P ligands / Ruthenium / Kinetics / Magnetic properties

The kinetic parameters for the axial-ligand-substitution reactions of $[Ru_2(\mu\text{-}O_2CCH_3)_4(MeCN)_2]^+$ in acetonitrile (MeCN) with PCy_3 and PCy_2Ph (Cy = cyclohexyl and Ph = phenyl) were investigated under pseudo first-order conditions of excess phosphane. The rate-determining formation of $[Ru_2(\mu\text{-}O_2CCH_3)_4(MeCN)(PCy_2R]^+$ appears independent of the nature of the incoming phosphane with an average k_1 (25.0 °C) = $(1.25 \pm 0.06) \times 10^3$ $M^{-1} s^{-1}$. A dissociatively activated mechanism is proposed for substitution of the axially coordinated acetonitrile, and the rate parameters are compared to earlier measurements carried out on $[Rh_2(\mu\text{-}O_2CCH_3)_4(MeCN)_2]$. Variable-temperature magnetic susceptibility measurements were carried out on the two phosphane diadducts, $[Ru_2(\mu\text{-}O_2CCH_3)_4(PCy_3)_2]PF_6$, (**1**) and $[Ru_2(\mu\text{-}O_2CCH_3)_4(PCy_2Ph)_2]PF_6$ (**2**), and showed behaviour unique to a Boltzmann distribution of states over the temperature range 2–300 K. To support the magnetic measurements, the single-crystal X-ray structure of **1** was redetermined at various temperatures down to –150 °C and showed a distinct decrease in the Ru–Ru bond length with decreasing temperature, consistent with a $\sigma^2\pi^4\delta^2\pi^{*3}$ configuration at low temperature (ground state) and a $\sigma^2\pi^4\delta^2\pi^{*2}\delta^{*1}$ configuration at room temp. In addition, the structure redeterminations of **1** were better resolved than the earlier reported structure and also corrected a minor error in that the molecule of solvation was found to be 1,2-dichloroethane instead of dichloromethane.

Introduction

Diruthenium tetracarboxylates, both in their homovalent $Ru_2(II,II)$ and valent-averaged $Ru_2(II,III)$ forms, have received considerable attention in the past 20 years owing primarily to their interesting electronic and magnetic properties.[1–4] The basic diruthenium tetracarboxylate "building block", $[Ru_2(\mu\text{-}O_2CR)_4]^{+/0}$, has been modified in a wide variety of ways leading to compounds with mesomorphic, catalytic and cytotoxic properties. Numerous extended polymeric and network structures based on these building blocks have also been assembled and display properties ranging from gas-occlusion[5–7] to ferrimagnetic ordering[8,9] and significant electronic delocalization.[10]

We recently reported the structure and electrochemistry of the first axial phosphane diadduct of diruthenium(II,III) tetraacetate.[11] We were able to isolate and crystallographically characterize what, in essence, was a kinetic product, $[Ru_2(\mu\text{-}O_2CCH_3)_4(PCy_3)_2]PF_6$ (**1**), by using the bulky phosphane, PCy_3 (Cy = cyclohexyl), which has a Tolman cone angle of 170°.[12] The bulkiness of the phosphane slowed down its thermodynamically favoured migration to the equatorial positions and subsequent displacement of the carboxylate groups. This process eventually leads to Ru–Ru bond cleavage and a total disassembly of the dimer into mononuclear fragments.[13] The structure revealed the longest Ru–Ru bond length in a diruthenium tetracarboxylate to date at 2.427(1) Å. In addition, we were able to generate, by cyclic voltammetry, the one-electron oxidation product, $[Ru_2(\mu\text{-}O_2CCH_3)_4(PCy_3)_2]^{2+}$, in which we have a $Ru_2(III,III)$ core. This is unprecedented for any diruthenium *tetracarboxylate*. Unfortunately we have, to date, not been able to isolate X-ray quality crystals of this oxidized species.

The extraordinarily long Ru–Ru bond length, as well as a small but significant redshift in the $\pi^*(Ru_2)\leftarrow\pi(RuO,Ru_2)$ visible transition when the phosphane diadduct is formed, motivated us to study both the variable-temperature magnetic susceptibility behaviour and the ligand substitution kinetics of complex **1** as well as those of the related complex, $[Ru_2(\mu\text{-}O_2CCH_3)_4(PPhCy_2)_2]PF_6$ (**2**). In addition, we have redetermined the structure of **1** at various temperatures in order to be able to correlate the Ru–Ru bond length/temperature dependence with the magnetic behaviour. The re-

[a] Department of Chemistry, St. Francis Xavier University, P. O. Box 5000, Antigonish, Nova Scotia B2G 2W5, Canada
Fax: +1-902-867-2414
E-mail: maquino@stfx.ca
[b] Department of Chemistry, Dalhousie University, Halifax, Nova Scotia B3H 4J3, Canada
[c] Department of Chemistry, Queen's University, Kingston, Ontario K7L 3N6, Canada
[d] Department of Chemistry, Memorial University of Newfoundland, St. John's, Newfoundland A1B 3X7, Canada
Supporting information for this article is available on the WWW under http://www.eurjic.org or from the author.

determination also corrects a minor mistake in the earlier structural formulation, replacing the original dichloromethane (DCM) of solvation with 1,2-dichloroethane (DCE). We report here as well the fully corrected structure, determined at –150 °C.

Results and Discussion

Synthesis

We found that the reaction of $[Ru_2(\mu\text{-}O_2CCH_3)_4(H_2O)_2]^+$, in which we exchanged the axial waters with modest and strong π-acid ligands, must be carried out stoichiometrically and reasonably fast. This is due to the fact that any excess of ligand or reaction times greater than 10 min will result in decomposition (disassembly) of the diruthenium core, which would lead to mononuclear ruthenium(II) complexes or a disproportionation reaction leading to a μ-oxido Ru_2(III,III) dimer and mononuclear Ru^{II} complex. These reactions have been seen, and exploited, by our group and others.[13,14] In a previous paper we synthesized a series of diadducts with modest π-acid N-heterocycles, $[Ru_2(\mu\text{-}O_2CCH_3)_4(\text{N-heterocycle})_2]^+$, by a rapid reaction of the diaqua adduct and 2 equiv. of the appropriate N-heterocycle in 2-propanol.[15] This reaction gave rapid precipitation of the desired product, which we were able to isolate, usually within 10 min.

We applied a similar strategy in trying to isolate adducts with the stronger π-acid phosphane ligands. It appears that for the reactions with phosphanes, PPh_3 in particular, a relatively rapid disproportionation occurs even when a relatively small excess of phosphane is employed.[14] The phosphane initially binds at the axial site and then performs an intramolecular migration to the equatorial positions leading to carboxylate displacement and Ru–Ru bond rupture. In our preliminary paper[11] we were able to somewhat slow down this migration process by using a significantly bulkier phosphane, PCy_3 (Cy = cyclohexyl), and hence we were able to isolate, purify and structurally characterize this diadduct. The electrochemistry was also reported. The detailed synthesis of this complex is given here. The bulkiness of the phosphane evidently slowed the axial–equatorial migration enough to allow us to isolate the diadduct. We can gauge the bulkiness of the phosphanes by looking at their Tolman cone angles.[12] For PPh_3, the angle is 145°, whereas for PCy_3, it is 170°. We also attempted to synthesize the PPh_3 diadduct along with diadducts involving phosphanes of intermediate cone angle, namely PPh_2Cy (cone angle = 153°) and $PPhCy_2$ (cone angle = 162°). In all three cases we were able to obtain some solid products; however, the PPh_3 and PPh_2Cy "products" gave very inconsistent elemental analyses, IR spectra and electrochemistry and could not be purified further, either by column chromatography or recrystallization, without appreciable decomposition. The $PPhCy_2$ reaction product **2** was more promising, and we were able to get reproducible analyses and spectra; however, X-ray quality crystals are still elusive.

The elemental analyses for adducts **1** and **2** are consistent with the formulations given. The IR spectra showed characteristic C–H stretching modes (primarily from the phenyl and cyclohexyl rings) in the range 2850–3070 cm^{-1}, asymmetric O–C–O stretching at 1440 cm^{-1}, symmetric O–C–O stretching at ≈ 1350 cm^{-1}, P–F stretching (from the PF_6^- counterion) at ≈ 840 cm^{-1} and the C–CH_3 bending mode at 692 cm^{-1}. The UV/Vis spectra were similar to the diaqua adduct except for a small bathochromic shift in the $\pi^*(Ru_2)\leftarrow\pi(RuO,Ru_2)$ band, a shift from 430 nm (in the diaqua complex) to 473 nm in **1** and 478 nm in **2** (Supporting Information, Figure S1).

Ligand Substitution Kinetics

The redshifting of the $\pi^*(Ru_2)\leftarrow\pi(RuO,Ru_2)$ band in **1** and **2** allowed us to monitor the ligand substitution process using stopped-flow techniques at 475 nm in dry acetonitrile (0.100 M $TBAPF_6$). Owing to our inability to differentiate exactly the λ_{max} value of the mono- from the diphosphane adduct (and hence determine accurately the absorptivity coefficients, ε) and the inherent instability of the diphosphane adduct once it is formed (particularly at high phosphane concentrations), we were not able to calculate successive equilibrium constants with sufficient accuracy to report here. Despite this fact, we assumed, as was the case with phosphane substitution reactions on the dirhodium(II,II) core in $Rh_2(\mu\text{-}O_2CCH_3)_4L_2$ complexes,[16] that the process should be dissociative with the substitution of the first axial ligand being rate determining, the second phosphane substituting rapidly owing to the *trans* effect (i.e. $k_2 >> k_1$). The steps required for substitution by PCy_3 are outlined in Equations (1) and (2).

$$[Ru_2(O_2CCH_3)_4(MeCN)_2] + PCy_3 \underset{k_{-1}}{\overset{k_1}{\rightleftharpoons}} [Ru_2(O_2CCH_3)_4(MeCN)(PCy_3)] + MeCN \quad (1)$$

$$[Ru_2(O_2CCH_3)_4(MeCN)(PCy_3)] + PCy_3 \underset{k_{-2}}{\overset{k_2}{\rightleftharpoons}} [Ru_2(O_2CCH_3)_4(PCy_3)_2] + MeCN \quad (2)$$

The formation of $[Ru_2(\mu\text{-}O_2CCH_3)_4(PCy_3)_2]^+$ was therefore monitored and, under pseudo first-order reaction conditions of excess phosphane concentrations {concentration of $[Ru_2(O_2CCH_3)_4(MeCN)_2]^+$ is 5.08×10^{-4} M} the rate expression can be given as that shown in Equation (3).

$$d[Ru_2(O_2CCH_3)_4(PCy_3)_2]^+ / dt = k_{obs}[Ru_2(O_2CCH_3)_4(MeCN)_2]^+ \quad (3)$$

and $k_{obs} = k_1[PCy_3]$. It should be noted at this point that as soon as the diadduct is formed it begins to disassemble/disproportionate with the rate of disassembly increasing as the concentration of the phosphane increases. In fact, at high phosphane concentrations (>35 mM) this subsequent decay can be seen at the end of the stopped-flow trace. However, at none of the concentrations used here does this

slower decay interfere with the initial rapid pseudo first-order formation (phosphane binding axially). Plots of k_{obs} against phosphane concentration are linear for the reactions with each of the two phosphanes. The plot for PCy_3 is shown in Figure 1a and, from the slope of the line, a value of $k_1(25\,°C) = 1.29(3) \times 10^3\ M^{-1}s^{-1}$ ($R^2 = 0.9981$) is obtained. Measurements of k_{obs} at various temperatures at a constant concentration of PCy_3 yielded a reasonably linear ($R^2 = 0.9843$) Eyring plot (Figure 1b) from which the activation parameters $\Delta H^{\neq}$ and $\Delta S^{\neq}$ could be determined. Identical treatment was used for the substitution with $PPhCy_2$. The basic rate data are reported in Table 1 with the second-order rate constants and activation parameters summarized in Table 2.

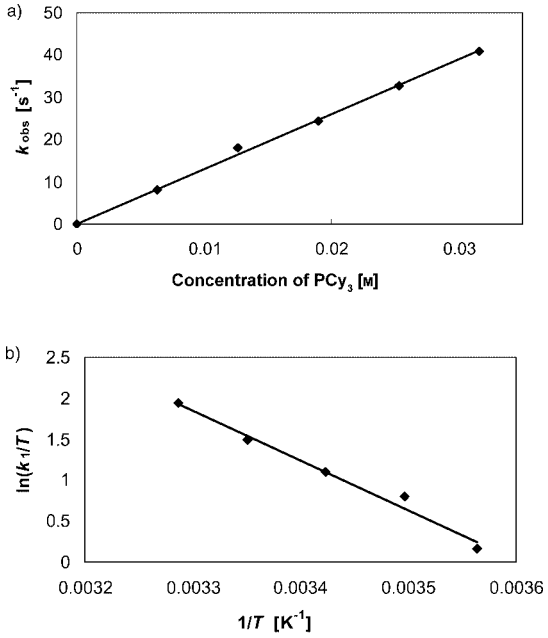

Figure 1. a) Plot of k_{obs} vs. [PCy_3] for the reaction of $[Ru_2(O_2CCH_3)_4(MeCN)_2]^+$ with PCy_3 in acetonitrile. b) Eyring plot for the reaction in a) with [PCy_3] = 0.0210 mM.

Table 1. Kinetic data for the reaction of $[Ru_2(\mu\text{-}O_2CCH_3)_4(MeCN)_2]^+$ with PCy_3 and $PPhCy_2$. Lig = PCy_3 or $PPhCy_2$.

T [°C]	[Lig] × 10^2 [M]	k_{obs} for PCy_3 [s^{-1}]	k_{obs} for $PPhCy_2$ [s^{-1}]	$k_1 \times 10^{-3}$ for PCy_3 [$M^{-1}s^{-1}$]	$k_1 \times 10^{-3}$ for $PPhCy_2$ [$M^{-1}s^{-1}$]
7.4	2.10	6.94	6.81	0.330(3)	0.325(2)
12.8	2.10	13.30	9.70	0.633(2)	0.462(3)
19.0	2.10	18.36	16.46	0.874(3)	0.784(3)
25.0	0.632	8.00	7.71	1.26(3)	1.22(4)
25.0	1.28	16.90	16.01	1.31(4)	1.25(2)
25.0	1.90	24.47	22.61	1.29(3)	1.19(4)
25.0	2.53	32.64	30.11	1.29(2)	1.19(3)
25.0	3.16	40.83	39.18	1.29(3)	1.24(3)
25.3	2.10	28.04	26.54	1.34(3)	1.26(4)
31.1	2.10	44.62	47.49	2.12(5)	2.26(6)

The rate law in Equation (3) implies that the formation of the monoadduct is the rate-determining step and that the redshifting of the $\pi^*(Ru_2) \leftarrow \pi(RuO,Ru_2)$ band is primarily due to the formation of $[Ru_2(\mu\text{-}O_2CCH_3)_4(PCy_3)(MeCN)]^+$, and the subsequent rapid formation of $[Ru_2(\mu\text{-}O_2CCH_3)_4(PCy_3)_2]^+$ causes little further change in the electronic spectrum. Because phosphanes lie higher than nitriles in the *trans* effect (and *trans* influence) series, a rapid second step would appear most likely. The Ru–P bond length in $[Ru_2(\mu\text{-}O_2CCH_3)_4(PCy_3)_2]^+$ is the longest of any Ru–L bond in complexes of this type, consistent with its *trans* influence. Unfortunately, attempts to measure the substitution of $[Ru_2(\mu\text{-}O_2CCH_3)_4(PCy_3)_2]^+$ with $PPhCy_2$ did not meet with any success as there was no noticeable change in the electronic spectrum.

Table 2. Rate and activation parameters for the substitution reactions of diruthenium(II,III) tetraacetate with PCy_3 and $PPhCy_2$ in acetonitrile and their comparison to similar reactions involving dirhodium(II,II) tetraacetate.

Ligand	k_1 [$M^{-1}s^{-1}$][a]	$\Delta H^{\neq}$ [kcal mol^{-1}]	$\Delta S^{\neq}$ [cal $K^{-1}mol^{-1}$]	Ref.
		Ru_2(II,III)		
PCy_3	$1.29(3) \times 10^3$	12.1(9)	–3.6(3.0)	[b]
$PPhCy_2$	$1.22(3) \times 10^3$	13.3(6)	0.3(2.3)	[b]
		Rh_2(II,II)		
PPh_3	$1.07(2) \times 10^5$	11.6(1)	3.4(4)	[16]
$P(OPh)_3$	$1.05(3) \times 10^5$	10.5(9)	–0.5(2.7)	[16]

[a] Measured at 25 °C. [b] This work.

Except for the *actual* value of the second-order rate constant, the substitution behaviour of the mixed-valent $[Ru_2(\mu\text{-}O_2CCH_3)_4(MeCN)_2]^+$ complex is remarkably similar to that of $[Rh_2(\mu\text{-}O_2CCH_3)_4(MeCN)_2]$.[16] The lack of dependence of k_1 on the nature of the phosphane would seem to imply a dissociatively activated formation of the monophosphane adduct. In addition, the highest occupied molecular orbitals (HOMO) of $[Ru_2(\mu\text{-}O_2CCH_3)_4(MeCN)_2]^+$ are the partially filled, near-degenerate, Ru–Ru-based $\pi^{*2}\delta^{*1}$. The electron density in these orbitals, which would be situated somewhere between the Ru–O(acetate) and Ru–L(axial ligand) bond axes, as well as the inherent steric bulk of the phosphanes, should prevent any significant associative attack by an incoming ligand. The activation parameters for the two complexes tell us little about the mechanism, the error in $\Delta S^{\neq}$ being too large to tell whether it is significantly positive (dissociative) or negative (associative).

The rate of axial ligand substitution (acetonitrile for phosphane) is two orders of magnitude slower in the present diruthenium system than in the aforementioned dirhodium complex. This can, presumably, be attributed to the higher charge on the metal centres (+2.5 in diruthenium vs. +2 in dirhodium) and the decreased number of antibonding electrons in the metal-centred HOMO (3 vs. 6).

Only one previous study dealt with ligand substitution in $[Ru_2(\mu\text{-}O_2CCH_3)_4L_2]^+$-type complexes. Dema and Bose[17] reported the anation reaction in acidic aqueous solution (pH = 1) of $[Ru_2(\mu\text{-}O_2CCH_3)_4(H_2O)_2]^+$ with Cl^-. They were able to determine successive equilibrium constants (K_1 = 15 M^{-1}, K_2 = 3.7 M^{-1}) because of the stability of the $[Ru_2(\mu\text{-}O_2CCH_3)_4Cl_2]^-$ diadduct and their ability to go to very high

concentrations of Cl^-, up to 2.0 M. Unfortunately, they were unable to measure the rates of anation, as more than 95% of the reaction was over in the time of mixing (4 ms) of their stopped-flow apparatus, which led them to estimate a lower limit for k_1 of $10^4\ M^{-1}s^{-1}$. This is not surprising (assuming a dissociative mechanism) as H_2O is a more labile leaving group than MeCN. Substitution rate constants of $Rh_2(\mu\text{-}O_2CCH_3)_4(H_2O)_2$ versus $Rh_2(\mu\text{-}O_2CCH_3)_4(MeCN)_2$ in most cases tend to be one or two orders of magnitude higher.[16,18]

Variable-Temperature Magnetic Susceptibility

Variable-temperature magnetic susceptibility measurements (2–300 K) were performed on complexes **1** and **2** as well as $[Ru_2(\mu\text{-}O_2CCH_3)_4(H_2O)_2]PF_6$. Figure 2 shows the plot of μ_{eff} vs. T for all three complexes. The plot for $[Ru_2(\mu\text{-}O_2CCH_3)_4(H_2O)_2]PF_6$ shows a decrease in μ_{eff} at low temperature owing to a large zero-field splitting parameter typical of many diruthenium complexes of this form.[4] We have fit the data to a model previously developed by Drago[19] and adapted by Maldivi and co-workers[20] to fit the magnetic data for $[Ru_2(\mu\text{-}O_2CCH_3)_4(H_2O)_2]BF_4$ (see ref[20] for details) and determined the g factor (g), zero-field splitting parameter (D) and temperature independent paramagnetism (TIP). The parameters obtained for our PF_6^- salt were $g = 2.186$, $D = 70.4\ cm^{-1}$ and TIP $< 10^{-6}\ cm^3\,mol^{-1}$ compared with $g = 2.190$, $D = 71.8\ cm^{-1}$ and TIP $< 10^{-6}\ cm^3\,mol^{-1}$ for the BF_4^- salt. This data is consistent with a ground-state configuration of $\sigma^2\pi^4\delta^2\pi^{*2}\delta^{*1}$, which displays significant zero-field splitting as the temperature is lowered, and the π* and δ* orbitals are essentially degenerate and often written as $(\pi^*\delta^*)^3$.

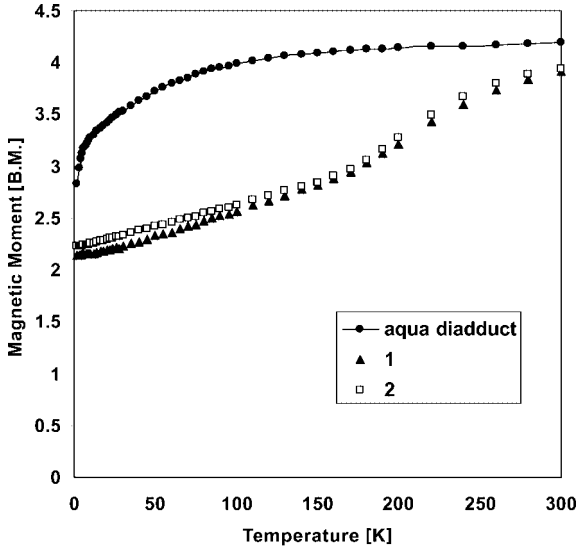

Figure 2. Plot of magnetic moment (B.M.) vs. temperature [K] for complexes **1**, **2** and $[Ru_2(\mu\text{-}O_2CCH_3)_4(H_2O)_2]PF_6$ (aqua diadduct).

The plots for **1** and **2** are quite similar to each other but distinctly different from the diaqua complex. In both cases the curves assume a sigmoidal shape with a long tail at low temperatures. The μ_{eff} value for **1** is 3.92 B.M. at 300 K (consistent with three unpaired electrons) and drops to 2.14 B.M. at 2 K (consistent with one unpaired electron), and similarly for **2**, the μ_{eff} is 3.94 B.M. at 300 K and 2.23 B.M. at 2 K. The shallow break in both curves occurs in the range 180–220 K. The values of μ_{eff} at 200 K are 3.22 B.M. for **1** and 3.27 B.M. for **2**, consistent with two unpaired electrons and a spin-crossover from an $S = 3/2$ to $S = 1/2$ state.

A wide variety of variable temperature magnetic behaviour has been ascribed to various diruthenium(II,III) complexes over the years: (1) high-spin (three unpaired electrons)[1–4] with ZFS (similar to the diaqua complex above), (2) low-spin (one unpaired electron),[21] (3) quantum mechanical spin admixed,[22] (4) Boltzmann distribution between π^{*3} and $\pi^{*2}\delta^*$ homoelectronic configurations[23] and (5) physical spin mixture.[24] From the temperature dependence and overall shape of our plots for complexes **1** and **2**, a Boltzmann distribution of configurations similar to what Cotton and co-workers[23] saw for the *para* isomer of the *N*,*N*′-diarylformamidinate derivative, $Ru_2(DArF)_4Cl$ with Ar = *p*-C_6H_4OMe, would seem reasonable. In this case, the π* orbital is somewhat more stable than the δ*, and one sees a Boltzmann distribution between the less stable $\pi^{*2}\delta^{*1}$ configuration (seen at room temp.) and the more stable π^{*3} configuration. Unfortunately, similar behaviour can also be ascribed to the situation where the δ* orbital is somewhat more stable than the π* orbital, and a Boltzmann distribution between the more stable $\delta^{*2}\pi^{*1}$ and less stable $\delta^{*1}\pi^{*2}$ occurs. To resolve the issue, Cotton looked at the structural changes that would need to take place for the two different Boltzmann distributions to be possible. When the π* orbital is more stable than the δ* orbital, a δ* electron is lost and a π* electron is gained as the temperature is lowered. Because a π* electron has a greater effect on the Ru–Ru bond than a δ* electron, the bond length will increase by 0.02–0.05 Å (on going from room temp. to 3 K). When the δ* orbital is more stable than the π* orbital, a δ* electron is gained at the expense of a π* electron, and the Ru–Ru bond length should decrease by 0.02–0.03 Å over the same temperature range.

In order to resolve this problem in our case we have redetermined the X-ray structure of **1** at various temperatures.

Redetermination of the X-ray Structure of Complex 1

The structure of **1** was redetermined at –150, –75, –60, –40, –25, –10, +20 and +50 °C. The redeterminations, performed on the same crystal we used in our earlier study,[11] were all better resolved than the original, and they also corrected an error in the nature of the molecule of solvation, with 1,2-dichloroethane replacing the dichloromethane (1,2-dichloroethane is often an impurity in dichloromethane). The new formulation is therefore $[Ru_2(\mu\text{-}O_2CCH_3)_4(PCy_3)_2]PF_6{\cdot}1,2\text{-}C_2H_4Cl_2$. Figure S2 (Supporting Information) shows the molecular structure, Table 3 gives the

crystal parameters and Table 4 includes selected bond lengths and angles for the structure redetermination of **1** at –150 °C.

Table 3. Crystal parameters for **1**·DCE at –150 °C.

Parameter	**1**·DCE
Empirical formula	$C_{46}H_{82}F_6O_8P_3Ru_2Cl_2$
Formula weight	1243.11
Crystal system	triclinic
Space group	$P\bar{1}$
T [K]	123.1(5)
a [Å]	10.5082(10)
b [Å]	11.4258(9)
c [Å]	12.6953(5)
α [°]	77.06(2)
β [°]	68.40(2)
γ [°]	71.33(2)
Volume [Å^3]	1332.8(2)
Z	1
$D_{calcd.}$ [g cm^{-1}]	1.549
μ [cm^{-1}]	8.26
F(000)	643
Crystal size [mm]	0.03 × 0.15 × 0.20
θ range [°]	3.2 to 72.4
Index ranges	$-26 \le h \le 20$ $-29 \le k \le 29$ $-26 \le l \le 31$
Collected reflections	63056
Independent reflections	39488 (R_{int} = 0.026)
Refinement method	full-matrix least squares on F^2
Data / restraints / parameters	7724 / 0 / 495
Goodness-of-fit on F^2	1.157
Final R values [$I > 2\sigma(I)$]	$R1$ = 0.026, $wR2$ = 0.070
R values (all data)	$R1$ = 0.027, $wR2$ = 0.070
Largest diff. peak/hole [e Å^{-3}]	0.49 / –0.71

Table 4. Selected bond lengths [Å] and angles [°] for **1**·DCE at –150 °C.

Ru(1)–Ru(1)	2.44222(15)	Ru(1)–P(1)	2.3445(5)
Ru(1)–O(1)	2.0320(12)	Ru(1)–O(2)	2.0128(7)
Ru(1)–O(3)	2.0645(12)	Ru(1)–O(4)	2.0930(8)
O(1)–C(19)	1.2693(18)	O(2)–C(21)	1.2735(15)
O(3)–C(19)	1.2721(14)	O(4)–C(21)	1.2668(15)
P(1)–C(1)	1.8515(16)	P(1)–C(7)	1.8433(10)
P(1)–C(13)	1.8627(12)	O(1)–C(19)	1.2693(18)
O(4)–C(21)	1.2668(15)	C(19)–C(20)	1.500(2)
C(21)–C(22)	1.4942(19)	C(1)–C(2)	1.5396(16)
Ru(1)–Ru(1)–P(1)	160.265(8)	Ru(1)–Ru(1)–O(1)	89.34(2)
Ru(1)–Ru(1)–O(2)	94.99(2)	Ru(1)–Ru(1)–O(3)	85.40(2)
Ru(1)–Ru(1)–O(4)	79.88(2)	P(1)–Ru(1)–O(1)	96.14(2)
P(1)–Ru(1)–O(2)	104.05(2)	P(1)–Ru(1)–O(3)	89.75(2)
P(1)–Ru(1)–O(4)	81.11(2)	O(1)–Ru(1)–O(2)	88.74(4)
O(1)–Ru(1)–O(3)	174.04(3)	O(1)–Ru(1)–O(4)	90.70(4)
O(2)–Ru(1)–O(3)	88.91(4)	O(2)–Ru(1)–O(4)	174.84(3)
O(3)–Ru(1)–O(4)	91.14(4)	Ru(1)–P(1)–C(1)	111.32(3)
Ru(1)–P(1)–C(7)	108.11(3)	Ru(1)–P(1)–C(13)	117.74(4)
C(1)–P(1)–C(7)	105.28(6)	C(1)–P(1)–C(13)	106.88(5)
C(7)–P(1)–C(13)	106.75(5)	Ru(1)–O(1)–C(19)	118.57(8)
Ru(1)–O(2)–C(21)	113.99(7)	Ru(1)–O(3)–C(19)	121.25(10)
Ru(1)–O(4)–C(21)	126.44(7)	O(1)–C(19)–O(3)	125.14(15)

All of the bond length and angle values for the redetermination at 20 °C are very similar to those of the earlier room temp. structure. For example, the redetermined bond length value for Ru–Ru is 2.42825(16) Å, for Ru–P it is 2.3717(4) Å and the Ru–Ru–P bond angle is 160.331(13)°. The values for the previous determination are 2.427(1) and 2.369(2) Å and 160.40(5)°, respectively.

Only two parameters, the Ru–Ru and Ru–P bond lengths, change significantly over the temperature range studied (50 to –150 °C) and this is shown in Figure 3. The Ru–Ru bond *increases* from 2.42373(15) Å at 50 °C to 2.44222(15) Å at –150 °C, a difference of +0.0185 Å. Despite the fact that we could not make measurements below –150 °C (123 K), this bond length *increase* is clearly significant and consistent with a π^{*3} configuration at low temperature and a $\pi^{*2}\delta^{*1}$ configuration at room temp., as concluded by Cotton. In addition, the Ru–P bond length *decreases* from 2.3735(4) Å at 50 °C to 2.3445(3) Å at –150 °C, a difference of –0.029 Å, indicative of increased back-donation from the now more populated Ru–Ru-based π* orbital to the phosphane.

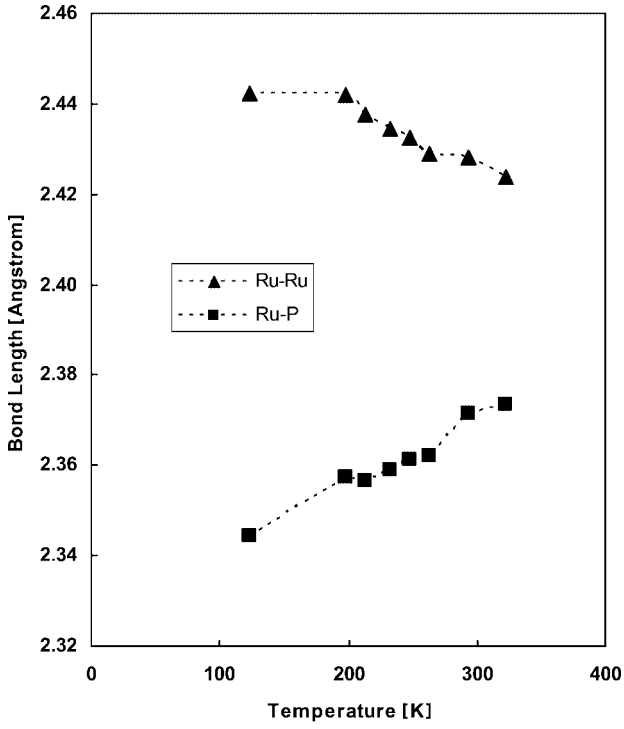

Figure 3. Plots of bond length vs. temperature for the Ru–Ru and Ru–P bonds in **1**.

It should be noted that no other major structural changes occur as the temperature is lowered. The space group is $P\bar{1}$ at all temperatures measured, and the unit cell volume contracts by about 3.7% over the range 50 °C to –150 °C, which is consistent with normal unit cell contraction as the temperature is lowered.

Conclusions

In this paper we reported the rate constants and activation parameters for the axial-ligand-substitution reactions of $[Ru_2(\mu\text{-}O_2CCH_3)_4(MeCN)_2]^+$ with the phosphanes PCy_3 and PCy_2Ph. This is the first time rate constants were

measured for any substitution reaction on the $[Ru_2(\mu\text{-}O_2CR)_4L_2]^+$ core. The rate constants are found to be about two orders of magnitude less than similar axial-ligand substitutions on the $[Rh_2(\mu\text{-}O_2CR)_4L_2]$ core. The two phosphane diadducts thus formed, $[Ru_2(\mu\text{-}O_2CCH_3)_4(PCy_3)_2]PF_6$ (**1**) and $[Ru_2(\mu\text{-}O_2CCH_3)_4(PCy_2Ph)_2]PF_6$ (**2**) were further investigated for their variable-temperature magnetic susceptibility properties and both displayed behaviour consistent with a Boltzmann distribution between a low temperature $\sigma^2\pi^4\delta^2\pi^{*3}$ doublet (ground-state) and a high temperature $\sigma^2\pi^4\delta^2\pi^{*2}\delta^{*1}$ quartet state. This conclusion is supported by the variable-temperature X-ray diffraction data of complex **1**, which shows an increase in the Ru–Ru bond length upon decreasing temperature, which is consistent with a metal–metal centred π* orbital being populated at the expense of a δ* orbital. Whereas Jiménez-Aparicio and co-workers[22] showed that the variation of the axial ligand in $[Ru_2(\mu\text{-}O_2CCH_3)(\mu\text{-}DPhF)_3X](BF_4)_n$-type systems ($DPhF^-$ = *N*,*N*′-diphenylformamidinate) can lead to high-spin (X = Cl^-, *n* = 0), low-spin (X = SCN^-, *n* = 0) or spin-admixed (X = H_2O, *n* = 1) complexes, Cotton and co-workers[23] showed that the variation of the equatorial ligand in $Ru_2(\mu\text{-}DArF)_4Cl$ systems ($DArF^-$ = *N*,*N*′-diarylformamidinate) can lead to a high-spin (Ar = *m*-C_6H_4OMe) complex or one showing a Boltzmann distribution of states (Ar = *p*-C_6H_4OMe); ours is the first example of a Boltzmann distribution being induced in a diruthenium(II,III) paddle-wheel-style complex by the variation of the *axial* ligand.

Experimental Section

General Remarks: Unless otherwise indicated all reactions were carried out under an inert (Ar) atmosphere. Tricyclohexylphosphane, PCy_3, and dicyclohexylphenylphosphane, $PPhCy_2$, were obtained from Aldrich and used as received. $[Ru_2(\mu\text{-}O_2CCH_3)_4(H_2O)_2]PF_6$ was prepared by a literature procedure.[25] IR spectra were recorded as KBr discs with a Bio-Rad FTS-175 spectrophotometer. UV/Vis spectra were recorded in 1-cm Hellma quartz cells with a Varian 100 spectrometer. C, H and P elemental analyses were performed by Canadian Microanalytical Service Ltd., Delta, BC, Canada. The variable temperature magnetic susceptibility data were recorded with a Quantum Design MPMS5S2 Superconducting Quantum Interference Device (SQUID) susceptometer at Memorial University over a temperature range of 2 to 300 K. Corrections for the diamagnetic contribution to the susceptibility of the samples and sample holder were performed on the raw data. The molar diamagnetic corrections for the complexes were calculated on the basis of Pascal's constants. The kinetics measurements were performed in acetonitrile with 0.100 M tetrabutylammonium hexafluorophosphate ($TBAPF_6$) with a SX-17MV stopped-flow spectrophotometer (Applied Photophysics), and the kinetic traces were fit to first-order reactions (4–6 replicate runs) by using the Applied Photophysics software on an Acorn A5000 workstation. The temperature was maintained at ±0.1 °C over the temperature range of 7–32 °C by using an external circulating water bath (VWR Scientific Model 1166).

$[Ru_2(\mu\text{-}O_2CCH_3)_4(PCy_3)_2]PF_6$ (1): A brief outline of this synthesis was reported earlier.[11] $[Ru_2(\mu\text{-}O_2CCH_3)_4(H_2O)_2]PF_6$ (0.100 g, 0.16 mmol) was dissolved in 2-propanol (7 mL). A solution of tricyclohexylphosphane (0.090 g, 0.32 mmol) in 2-propanol (3 mL) was added, with stirring, at room temp. and allowed to react for no more than 5 min. The dark brown precipitate that formed was immediately filtered off in vacuo and washed with 2-propanol (30 mL) after which it was dried in vacuo. Crystals could be grown under an atmosphere of argon by rapid evaporation from DCM. Yield: 0.15 g (80%). IR (KBr): $\tilde{\nu}$ = 2931 (s), 2854 (s), 1440 (s), 1345 (s), 1271 (m), 1113 (m), 1005 (m), 843 (s), 731 (m), 692 (s), 558 (m), 510 (m) cm^{-1}. UV/Vis (1,2-dichloroethane): λ (ε, $L\,mol^{-1}\,cm^{-1}$) = 473 (≈ 900) nm. $C_{44}H_{78}F_6O_8P_3Ru_2$ (1144.58): calcd. C 46.17, H 6.87, P 8.12; found C 45.84, H 6.55, P 8.08.

$[Ru_2(\mu\text{-}O_2CCH_3)_4(PPhCy_2)_2]PF_6$ (2): This diadduct was prepared in a similar fashion to **1** except that dicyclohexylphenylphosphane (0.088 g, 0.32 mmol) was used. Yield: 0.15 g (81%). IR (KBr): $\tilde{\nu}$ = 3064 (w), 2931 (s), 2852 (s), 1440 (s), 1355 (s), 1274 (m), 1189 (m), 1112 (m), 1003 (m), 843 (s), 692 (s), 558 (m) cm^{-1}. UV/Vis (1,2-dichloroethane): λ (ε, $L\,mol^{-1}\,cm^{-1}$) = 479 (≈ 900) nm. $C_{44}H_{66}F_6O_8P_3Ru_2$ (1132.05): calcd. C 46.68, H 5.88, P 8.21; found C 46.84, H 6.13, P 8.01.

X-ray Crystallographic Study: All measurements were made with a Rigaku RAXIS RAPID imaging plate area detector with graphite monochromated Mo-K_α radiation. Indexing was performed from 4 oscillations that were exposed for 600 seconds. The data were collected at temperatures of (–150, –75, –60, –40, –25, –10, +20 and +50) ± 0.5 °C to a maximum 2θ value of 145.2 °. The crystal-to-detector distance was 127.40 mm. Readout was performed in the 0.100 mm pixel mode. The data were corrected for Lorentz and polarization effects. A correction for secondary extinction was applied.[26] The structures were solved by direct methods[27] and expanded by using Fourier techniques.[28] The non-hydrogen atoms were refined anisotropically. Some hydrogen atoms were refined isotropically and the rest were refined by using the riding model. The final cycle of full-matrix least-squares refinement was on F^2.

Neutral atom scattering factors were taken from Cromer and Waber.[29] Anomalous dispersion effects were included in $F_{calcd.}$;[30] the values for $\Delta f'$ and $\Delta f''$ were those of Creagh and McAuley.[31] The values for the mass attenuation coefficients are those of Creagh and Hubbell.[32] All calculations were performed by using the CrystalStructure[33–34] crystallographic software package except for the refinement, which was performed with SHELXL-97.[35] CCDC-640710 to -640717 (for **1** at the various temperatures) contain the supplementary crystallographic data for this paper. These data can be obtained free of charge from The Cambridge Crystallographic Data Centre via www.ccdc.cam.ac.uk/data_request/cif.

Supporting Information (see footnote on the first page of this article): Electronic spectra of **1** and its precursor and the ORTEP diagram of $\mathbf{1}^+$.

Acknowledgments

M. A. S. A. acknowledges the Natural Sciences and Engineering Research Council (Canada) for financial support.

[1] M. A. S. Aquino, *Coord. Chem. Rev.* **1998**, *170*, 141–202.
[2] M. A. S. Aquino, *Coord. Chem. Rev.* **2004**, *248*, 1025–1045.
[3] F. A. Cotton, C. A. Murillo, R. A. Walton, *Multiple Bonds Between Metal Atoms*, 3rd ed., Springer Science and Business Media, New York, **2005**.
[4] M. Mikuriya, D. Yoshioka, M. Handa, *Coord. Chem. Rev.* **2006**, *250*, 2194–2211.

[5] S. Takamizawa, K. Yamaguchi, W. Mori, *Inorg. Chem. Commun.* **1998**, *1*, 177–178.
[6] S. Takamizawa, T. Ohmura, Y. Yamaguchi, W. Mori, *Mol. Cryst. Liq. Cryst.* **2000**, *342*, 199–204.
[7] T. Ohmura, W. Mori, H. Hiraga, M. Ono, Y. Nishimoto, *Chem. Lett.* **2003**, *32*, 468–469.
[8] Y. Liao, W. W. Shum, J. S. Miller, *J. Am. Chem. Soc.* **2002**, *124*, 9336–9337.
[9] D. Yoshioka, M. Mikuriya, M. Handa, *Chem. Lett.* **2002**, 1044–1045.
[10] H. Miyasaka, C. S. Campos-Fernández, R. Clérac, K. R. Dunbar, *Angew. Chem. Int. Ed.* **2000**, *39*, 3831–3835.
[11] G. G. Briand, M. W. Cooke, T. S. Cameron, H. M. Farrell, T. J. Burchell, M. A. S. Aquino, *Inorg. Chem.* **2001**, *40*, 3267–3268.
[12] C. A. Tolman, *Chem. Rev.* **1977**, *77*, 313–348.
[13] I. W. Wyman, T. J. Burchell, K. N. Robertson, T. S. Cameron, M. A. S. Aquino, *Organometallics* **2004**, *23*, 5353–5364.
[14] M. C. Barral, R. Jiménez-Aparicio, E. C. Royer, F. A. Urbanos, A. Monge, C. Ruiz-Valero, *Polyhedron* **1991**, *10*, 113–120.
[15] G. Vamvounis, J. F. Caplan, T. S. Cameron, K. N. Robertson, M. A. S. Aquino, *Inorg. Chim. Acta* **2000**, *304*, 87–98.
[16] M. A. S. Aquino, D. H. Macartney, *Inorg. Chem.* **1987**, *26*, 2696–2699.
[17] A. C. Dema, R. N. Bose, *Inorg. Chem.* **1989**, *28*, 2711–2713.
[18] K. Das, E. L. Simmons, J. L. Bear, *Inorg. Chem.* **1977**, *16*, 1268–1271.
[19] J. Telser, R. S. Drago, *Inorg. Chem.* **1984**, *23*, 3114–3120.
[20] F. D. Cukiernik, A.-M. Giroud-Godquin, P. Maldivi, J.-C. Marchon, *Inorg. Chim. Acta* **1994**, *215*, 203–207.
[21] M. C. Barral, R. González-Prieto, S. Herrero, R. Jiménez-Aparicio, J. L. Priego, E. C. Royer, M. R. Torres, F. A. Urbanos, *Polyhedron* **2004**, *23*, 2637–2644.
[22] M. C. Barral, S. Herrero, R. Jiménez-Aparicio, M. R. Torres, F. A. Urbanos, *Angew. Chem. Int. Ed.* **2005**, *44*, 305–307.
[23] P. Angaridis, F. A. Cotton, C. A. Murillo, D. Villagrán, X. Wang, *J. Am. Chem. Soc.* **2005**, *127*, 5008–5009.
[24] M. C. Barral, T. Gallo, S. Herrero, R. Jiménez-Aparicio, M. R. Torres, F. A. Urbanos, *Inorg. Chem.* **2006**, *45*, 3639–3647.
[25] K. D. Drysdale, E. J. Beck, T. S. Cameron, K. N. Robertson, M. A. S. Aquino, *Inorg. Chim. Acta* **1997**, *256*, 243–252.
[26] A. C. Larson in *Crystallographic Computing* (Ed.: F. R. Ahmed), Munksgaard, Copenhagen, **1970**, pp. 291–294.
[27] *SIR92*: A. Altomare, G. Cascarano, C. Giacovazzo, A. Guagliardi, M. Burla, G. Polidori, M. Camalli, *J. Appl. Cryst.* **1994**, *27*, 435.
[28] *DIRDIF99*: P. T. Beurskens, G. Admiraal, G. Beurskens, W. P. Bosman, R. de Gelder, R. Israel, J. M. M. Smits, *The DIRDIF-99 Program System*, Technical Report of the Crystallography Laboratory, University of Nijmegen, The Netherlands, **1999**.
[29] D. T. Cromer, J. T. Waber, *International Tables for X-ray Crystallography*, The Kynoch Press, Birmingham, England, **1974**, vol. IV, Table 2.2A.
[30] J. A. Ibers, W. C. Hamilton, *Acta Crystallogr.* **1964**, *17*, 781–782.
[31] D. C. Creagh, W.J McAuley, *International Tables for Crystallography* (Ed.: A. J. C. Wilson), Kluwer Academic Publishers, Boston, **1992**, vol. C, Table 4.2.6.8, pp. 219–222.
[32] D. C. Creagh, J. H. Hubbell, *International Tables for Crystallography* (Ed.: A. J. C. Wilson), Kluwer Academic Publishers, Boston, **1992**, vol. C, Table 4.2.4.3, pp. 200–206.
[33] *CrystalStructure 3.6.0*: *Crystal Structure Analysis Package*, Rigaku and Rigaku/MSC, 9009 New Trails Dr., The Woodlands, TX, 77381 USA, **2000**–**2004**.
[34] *CRYSTALS Issue 10*: D. J. Watkin, C. K. Prout, J. R. Carruthers, P. W. Betteridge, Chemical Crystallography Laboratory, Oxford, UK, **1996**.
[35] G. M. Sheldrick, *SHELXL97*, University of Göttingen, **1997**.

Received: April 11, 2007
Published Online: July 6, 2007

